Eur. Phys. J. B **55**, 411–418 (2007)
DOI: 10.1140/epjb/e2007-00081-y

THE EUROPEAN PHYSICAL JOURNAL B

Thermally induced effects on the diffraction pattern of a dye doped nematic film

R.F. Rodríguez[1,a,b], J.A. Reyes[1,b], J. Fujioka[2,b], E. Cortés[1,b,c], J.A. Olivares[3,b], and F.L.S. Cuppo[3]

[1] Departamento de Física Química, Instituto de Física, Universidad Nacional Autónoma de México, Apdo. Postal 20–364, 01000 México, D. F., México
[2] Departamento de Materia Condensada, Instituto de Física, Universidad Nacional Autónoma de México, Apdo. Postal 20–364, 01000 México, D. F., México
[3] Centro de Investigación en Polímeros, COMEX, Marcos Lobatón No. 2, 55885 Tepexpan, Edo. de México, México

Received 12 December 2006
Published online 22 March 2007 –

Abstract. We investigate the effects produced on the diffraction pattern of a dyed nematic thin film under the action of an optical field and a low frequency AC electric field. For a homeotropically aligned mixture of the nematic $E7$ doped with a dichroic dye, a sequence of dynamical regimes of the far field diffraction pattern is observed. For specific values of the beam's power, frequency and amplitude of the AC field, a uniform steady rotational motion (SR) of the pattern sets in with a measured angular velocity $\nu_{exp} = 2.58$ Hz. To account for this and other observed features of the diffraction pattern an analytical model is proposed. This allows us to describe quantitatively the reorientation of the film, to calculate some specific structural features of the diffraction pattern, as well as its angular velocity. We find that the predicted angular velocity $\nu_{theor} = 5.7$ Hz, is in quite good agreement with the measured value.

PACS. 78.20.Nv Thermooptical and photothermal effects – 61.30.Gd Orientational order of liquid crystals; electric and magnetic field effects on order – 42.65.-k Nonlinear optics

1 Introduction

An intense light wave propagating through a nematic liquid crystal cell (NC) may strongly alter its local optical properties and may induce a variety of optical responses of the fluid. In particular, the far field diffraction pattern produced by a thin, pure, nematic film has been studied since the early 80's. In pure nematics it is well known that an incident elliptically polarized beam may induce a variety of dynamic regimes in the polarization of the beam. These responses range from a regular motion of the director [1–4], to a sequence of torsional oscillations, rotations, nutation with precession and other phenomena [5–7]. The response may also be a complex and chaotic dynamics of the director [8]. In addition to this variety of responses, it is also well established that the response of the film may be greatly enhanced by the addition of small amounts of dichroic dyes. This allows to observe highly nonlinear optical phenomena with moderate power light sources. However, even with the doping, the diffraction pattern of the NC has always been reported to remain stationary [7,9].

In recent work we have extended the scope of these experiments in two ways [10,11]: first, by doping the nematic with an azoic ink and secondly, by applying a low frequency electric AC field across the cell plates, in addition to the incident linearly polarized laser beam. Under the combined action of these fields, the director's reorientation of the doped nematic film produced a diffraction pattern in the far field. It consisted of a countable set of thick rings around a central bright spot, but blurred in the periphery of the pattern. The nature of these observations and the details of the experimental set up were reported in more detail in references [10,11]. The important point to stress, though, is that in the presence of both fields the director's reorientation produced a diffraction pattern which exhibits a sequence of dynamic regimes existing for well defined threshold values of the beam's power, frequency, amplitude and root mean square voltage V_{rms} of the AC field [10].

In the present work we shall restrict ourselves to the analysis of one of these dynamic regimes, namely, the SR regime in which a uniform rotation of the pattern was observed. Our basic purpose here is to propose an analytical model that allows us to calculate a diffraction pattern

[a] e-mail: zepeda@fisica.unam.mx
[b] Fellow of SNI, Mexico.
[c] On sabbatical stay. *Permanent address*: Departamento de Física, Universidad Autónoma Metropolitana-Iztapalapa, Apdo. Postal 55-534, México D.F. 09340, Mexico.

possessing some of the qualitative and quantitative features of the experimental observations. More specifically, as will be shown later on, the proposed model describes the appearance of a rotating structure and predicts an angular velocity which agrees quite well with the measured one. To this end the article is organized as follows. In Section 2, we briefly review those features of the observations that are relevant for our purpose in this work. Then we introduce the model and we argue that the space-time variation of the reorientation of the nematic is coupled to the heating of the NC through the gradient of the order parameter of the nematic. We introduce a heating model which leads to a steady-state temperature equation which can be solved exactly in analytical form. However, as is discussed in Section 3, it is sufficient to work with an approximate temperature profile as a function of the distance from the center of the beam. We then use this approximate profile to obtain an analytical solution to the reorientation equation. For this purpose it will be shown that these solutions exhibit two of the features of the observed diffraction pattern, namely, the nearly circular rings and the rotating blurred structure mentioned above. Then we calculate the angular velocity of rotation of the pattern from this solution and estimate its numerical value for typical values of the material and experimental parameters. We find a theoretical angular velocity, $\nu_{theo} = 5.7$ Hz which agrees quite well with the measured value of the same quantity, $\nu_{exp} = 2.58$ Hz. Finally, we close the paper by discussing the advantages and limitations of our approach and by making further critical remarks.

2 System and basic equations

To start with, we review those features of the observations in the SR regime that will be relevant in the formulation of the theoretical model. In the experiments we used a mixture of the nematic $E7$ doped with 0.5% Wt of $R4$ dye. This mixture was sandwiched between two ITO coated glass plates separated by 24 μm spacers. The glass plates were previously coated with lecithin to achieve a homeotropic alignment. Then, the NC was illuminated with a linearly polarized cw Ar laser at 514 nm in normal incidence configuration. The beam's transverse profile was Gaussian and it was focused on the sample with a $f = 100$ μm convergent lens which produced a beam's waist of $\sigma = 31$ μm at the focal plane. To control the input power a set of one half wave plates and a polarizer were used. A beam splitter was introduced into the path of the beam to monitor its power with a previously calibrated photodiode. By using a wave function generator an AC field with a frequency $\nu = 1$ kHz was applied to the sample perpendicularly to the plates, as depicted in Figure 1.

With the sample at the focal plane and in the absence of the AC field, the input power was slowly increased until an intensity of 6.45 mW was reached. At this power a pattern of blurred, thick, countable, but static diffraction rings around the central bright spot was observed. Actually, the blurring of the rings system is an indication

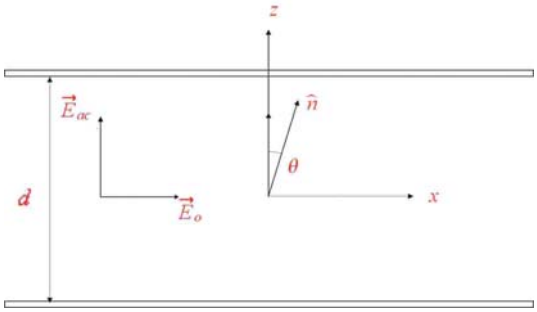

Fig. 1. Schematics of the NC and the applied fields.

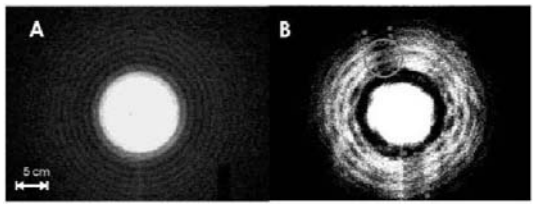

Fig. 2. The observed blurred rotating diffraction pattern for $P = 11.93$ mW and $\nu_{ac} = 1$ kHz. The circle identifies the maximum contrast region MCR.

of a melting process due to the formation of an isotropic droplet within the path of the laser beam [7,10,11]. Above this threshold the number of diffraction rings increased and they became thinner. However, during this processes the diffraction pattern remained static. When the AC field was connected at a fixed beam's power of $P = 11.93$ mW, the V_{rms} of the AC field was increased. It was expected that the rings would disappear at a definite V_{rms}, as it occurs with a pure substance, however, instead it was observed that for $V_{rms} = 17.37$ V, a steady rotational (SR) uniform motion of the pattern sets in. This observation suggests that the presence of both fields produces a competition of the torques they produce for the chosen geometry, and that this competition prevents the reorientation of the director until the threshold value is attained. The number of rings remained constant and a tenuous blurred rotating vane-structure around the bright central spot and superposed to the ring pattern, was also observed. However, the pattern of nearly circular rings started to rotate with a steady counterclockwise rotational uniform motion which could be followed at the naked eye. These deformed fringes produced a region of maximum contrast (MCR) where the intensity is a maximum in comparison with the surrounding fringes, as shown in Figure 2.

Focusing on the MCR, its average angular velocity was measured by placing a photodetector behind a hole of a 2 mm diameter and at a distance of 30 mm from the center of the screen. The angular velocity of this rotating shadowy structure was measured by analyzing each frame of a recorded sequence yielding a value of $\nu_{exp} = 2.58$ Hz. If these features are maintained until the V_{rms} reaches the threshold value $V_{rms} = 26.02$ V, the dynamic regime becomes unstable. Then the angular velocity is no longer constant and in some cases the spinning sense even changes abruptly to the clockwise

direction. Above this threshold other dynamic regimes set in and some of their features are discussed in more detail in references [10,11].

2.1 Model

The Gaussian laser beam which is linearly polarized along the $\widehat{x}$-axis, propagates along the $\widehat{z}$ direction and incides normally to the film, is of the form

$$\boldsymbol{E}_{opt} = E_o e^{-(r/\sqrt{2}\sigma)^2 + i(zk_z' - \omega_o t)} e^{-zk_z'' - \alpha_\perp r}\hat{x}. \quad (1)$$

Here E_o is the on axis amplitude, r denotes the distance from the optical axis of the beam, $\sqrt{2}\sigma$ represents the radius of the beam's waist, ω_o stands for its frequency and $\hat{x}$ denotes the unit vector along the x-axis. k_z' and k_z'' are, respectively, the real and imaginary parts of the wave vector k_z along the z-axis; $k_z'' \equiv \alpha_\perp$describes the absorption of the beam by the medium. The component of the absorption coefficient of the dye along the radial direction is given by $\alpha_\perp$. As a consequence, the intensity at a point (r, z) is given by

$$I(r,z) \equiv \mid \boldsymbol{E}_{opt} \mid^2 = \frac{P}{\pi\omega_o^2} e^{-\frac{r^2}{\omega_o^2} - 2\alpha_\perp z}, \quad (2)$$

since $\frac{r^2}{\sigma^2} \gg 2\alpha_\perp r$ and where P is the input power.

On the other hand, the AC field is of the form

$$\boldsymbol{E}_{ac} = E_s e^{i\omega_{ac}t}\hat{z}, \quad (3)$$

where its amplitude $E_s \equiv V_{rms}/d$ is defined in terms of the root mean square voltage, V_{rms}, across the cell of width d; ω_{ac} denotes the angular frequency, $\hat{z}$ is the unit vector along the z-axis and $i = \sqrt{-1}$. If the polarization of the optical field remains in the $x-z$ plane, it is reasonable to assume that the reorientation of the director will also take place in the same plane. Thus, if we further assume strong anchoring boundary conditions for the director at the plates, the director field $\hat{n}$ will be

$$\hat{n} = (n_x, 0, n_z) = [\sin\theta(r,\phi,z,t), 0, \cos\theta(r,\phi,z,t)], \quad (4)$$

where θ is the reorientation angle which is a function of the cylindrical coordinates (r, ϕ, z).

The optical field gives rise to two main effects which are about two orders of magnitude larger than for a pure nematic, namely, it induces a torque that reorients the director and it produces a significant thermal heating, which changes the nonlinear part of the refractive index due to the large absorption coefficients of the dye. As mentioned earlier, the blurring of the rings in the observed pattern is an indication of a melting process, due to the formation of an isotropic droplet within the path of the laser beam. To verify this issue we carried out a pump-probe experiment. A linearly polarized second (probe) laser beam (He $-$ Ne, $\lambda = 636$ nm, $P_{\mathrm{He-Ne}} = 3$ mW), parallel to the pump beam, was also focused on the sample. By inserting a filter to block the green pump's beam, we observed a Fraunhoffer diffraction pattern characteristic of a circular aperture. If the polarization of the probe beam is changed by 90°, the pattern remains unchanged, indicating that it is produced by an isotropic droplet. The diameter of the probe beam was 19.95 μm and the diameter of the droplet was 21.89 μm at a power of 7.13 mW.

When the number of rings in the SR remains constant, we expect that the director, $\widehat{n}(\overrightarrow{r}, t)$, is aligned with the optical field. Furthermore, as it is well known in the guest-host effect [12], we also expect that the long axis of the dye molecules will be oriented in the same direction, if they are in their ground state. However, since the dye's dichroism is positive, the absorption along the direction of propagation of the beam (z) should be larger than along the transverse directions.

2.2 Heating model

Let us assume that the heating process induced by the beam reaches a steady-state whose temperature profile may be described by an equation of the form [13]

$$\nabla \cdot (\overleftrightarrow{\kappa} \cdot \nabla T) = -\alpha_\perp I(r,z), \quad (5)$$

where the heat conductivity tensor $\overleftrightarrow{\kappa}$ is of the form

$$\overleftrightarrow{\kappa} = \begin{pmatrix} \kappa_\perp & 0 & 0 \\ 0 & \kappa_\perp & 0 \\ 0 & 0 & \kappa_\parallel \end{pmatrix} \quad (6)$$

and $\kappa_\parallel$ and $\kappa_\perp$ are its parallel and perpendicular components. As boundary conditions we assume that the temperature and normal component of the heat flow are continuous at the substrate-nematic interfaces. The temperature dependence of both, the heat conductivities and the absorption coefficient $\alpha_\perp$ are neglected.

Note that if equation (1) is integrated over a volume V containing the whole beam and the width of the cell, it can be rewritten as

$$\kappa_\perp \left(\frac{\partial T}{\partial r}\right)_{r=0} + \kappa_\parallel \left(\frac{\partial T}{\partial z}\right)_{z=0} - \kappa_\parallel \left(\frac{\partial T}{\partial z}\right)_{z=d} = -\alpha_\perp \int_V I(r,z)dV, \quad (7)$$

which shows that the components of ∇T relevant to define the temperature profile are $\partial T/\partial r$ and $\partial T/\partial z$. However, inside the beam, i.e., for $r \leq \sigma$, the Gaussian profile of the beam implies that

$$\frac{\partial T}{\partial z} \ll \frac{\partial T}{\partial r}, \quad r \leq \sigma, \quad (8)$$

whereas for $r \geq \sigma$,

$$\frac{\partial T}{\partial z} \gg \frac{\partial T}{\partial r}. \quad (9)$$

Now, for the geometry under consideration equation (5) reads

$$\kappa_\perp \left(\frac{\partial^2 T}{\partial r^2} + \frac{1}{r}\frac{\partial T}{\partial r}\right) + \kappa_\parallel \frac{\partial^2 T}{\partial z^2} - \alpha_\perp I(r,z). \quad (10)$$

By following the method proposed in references [13,14], to solve equations of this form, the temperature rise can be described analytically in terms of the Hankel-transformation of the temperature field

$$T(r,z) \equiv \int_0^\infty \lambda \widetilde{T}(\lambda,z) J_0(\lambda r) d\lambda, \tag{11}$$

as

$$\alpha_\perp^2 \kappa_\parallel \frac{\partial^2}{\partial z^2}\widetilde{T}(r,z) - \lambda^2 \kappa_\perp \widetilde{T}(r,z) = - \frac{P\alpha_\perp}{2\pi} e^{-\alpha_\perp z} e^{-\frac{\lambda^2\omega_o^2}{4}}, \tag{12}$$

where J_0 is the first order Bessel function. For the above mentioned boundary condition the solution of this equation reads

$$\widetilde{T}(\lambda,z) = \frac{P\alpha_\perp}{2\pi\kappa_\perp} \frac{e^{-\frac{\lambda^2\omega_o^2}{4}}}{\lambda^2 - (\alpha_\perp \xi)^2} \times \left(e^{-\alpha_\perp z} + G_1 e^{\frac{\lambda z}{\xi}} + G_2 e^{-\frac{\lambda z}{\xi}} \right), \tag{13}$$

where we have used the following abbreviations $\xi \equiv \left(\frac{\kappa_\parallel}{\kappa_\perp}\right)^{1/2}$,

$$G_1 \equiv \frac{(1+k)\, e^{-\alpha_\perp d} + (1-k)\, e^{-\frac{\lambda d}{\xi}} (1 - \alpha_\perp \xi k/\lambda)}{(1+k)^2 e^{\frac{\lambda d}{\xi}} - (1-k)^2 e^{-\frac{\lambda d}{\xi}}}, \tag{14}$$

$$G_2 \equiv \frac{\alpha_\perp \xi k/d - 1}{(1+k)^3 e^{\frac{\lambda L}{\xi}}} \left\{ \left[(1+k)^2 e^{\frac{\lambda d}{\xi}} - (1-k)^2 e^{-\frac{\lambda d}{\xi}} \right] - (1-k) \left[(1+k)\, e^{-\alpha_\perp d} + (1+k)\,(1 - \alpha_\perp \xi k/\lambda)\, e^{-\frac{\lambda d}{\xi}} \right] \right\}, \tag{15}$$

and

$$k \equiv \frac{\sqrt[2]{\kappa_\parallel \kappa_\perp}}{\kappa_s}. \tag{16}$$

Although in principle it is possible to obtain an exact analytical expression for the temperature profile $T(r,z)$ by calculating the inverse transform of the function $\widetilde{T}(\lambda,z)$ given by equation (13), this calculation it is not easy to perform. However, it can be verified that a good approximation for the temperature profile just outside the beam for $z_o = 30$ μm, may be represented by

$$T_{app}(r,z_o) = \frac{A_1}{A_2 + r^2}, \tag{17}$$

where A_1 and A_2 are adjustable parameters, since the Hankel transform of this function, namely,

$$\widetilde{T}_{app}(\lambda,z_o) = A_1 K_0(A_2\lambda), \tag{18}$$

where $K_0(A_2\lambda)$ is the modified Bessel function of order zero, is close to the exact function $\widetilde{T}(\lambda,z_o)$ for $\lambda \sim 2\times 10^4$,

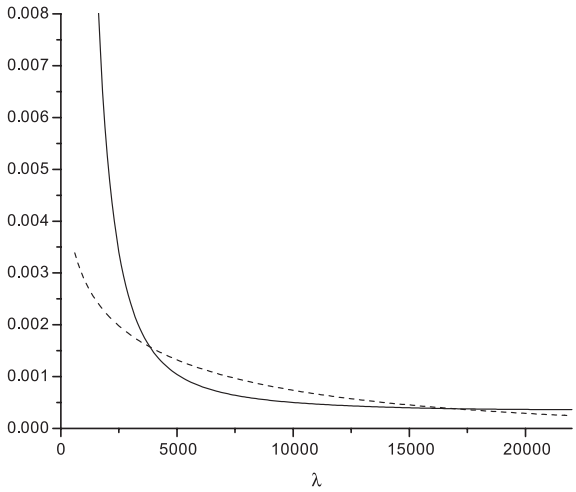

Fig. 3. $\widetilde{T}(\lambda,z_o)$ (—) and $\widetilde{T}_{app}(\lambda,z_o)$ (− − −) as functions of λ for $z_o = 30$ μm and for typical values of the material and experimental parameters.

which corresponds to distances of $2\pi/\lambda \sim 300$ μm which are clearly greater than σ. For example, if we take the following typical values of the required material and experimental parameters [11,10,13], namely, $P = 11.93$ mW, $\alpha_\perp = 2.57 \times 10^4$ m^{-1}, $\kappa_\perp = 10^{-1}$ W/°K m, $\kappa_\parallel = 2\kappa_\perp$, $\kappa_s = 3.7\kappa_\parallel$, $d = 24$ μm, $\sigma = 31$ μm, and if we set $A_1 = 10^{-3}$ ° K m^2 and $A_2 = 2 \times 10^{-6}$ m, the graphs of the functions $\widetilde{T}(\lambda,z_o)$ and $\widetilde{T}_{app}(\lambda,z_o)$ are, indeed, quite close to each other within the range $10^4 < \lambda < 2\times 10^4$, as shown in Figure 3.

3 Order polarization

A nematic liquid crystal is characterized by a tensorial order parameter $Q_{ij} = S\,(n_i n_j - \delta_{ij}/3)$ with modulus S. In connection with the problem of determining the orientation of $\widehat{n}$ at a nematic-isotropic interface, it has been suggested long ago that a gradient of S at constant $\widehat{n}$ may induce an electric polarization [15,16]. However, a more complete analysis of the connection between the order polarization and the spatial variations of S in liquid crystals was given more recently by Barbero et al. [17], who established how the surface orientation is related with the order polarization in the spontaneous tilted orientation at the nematic-isotropic interface. Then, on the one hand, we know that the existence of a temperature gradient generates a gradient of the scalar order parameter, namely, $\overrightarrow{\nabla S} \equiv \gamma \overrightarrow{\nabla T}$, [18,19], where $\gamma \equiv dS/dT$ is in general a function of r. On the other hand, the fact that in our system there is a nematic-isotropic interface which separates a tilted nematic state from the isotropic droplet, suggests to use Barbero et al theory to describe the effects of the heating on the order parameter and on the director´s orientation. With this approach in mind, we then may say that the temperature gradient induces a scalar order parameter gradient, approximately parallel to $\boldsymbol{E}_{opt}$, and which in turn generates an order electric polarization,

$\boldsymbol{P}_{ord}$. Taking into account (8), this polarization may then be written as

$$\boldsymbol{P}_{ord} \equiv f_0\gamma\left[\left(\hat{n}\cdot\frac{dT}{dr}\widehat{r}\right)\hat{n}-\frac{1}{3}\frac{dT}{dr}\widehat{r}\right], \tag{19}$$

where f_0 is the order effect coefficient [17] and $\widehat{r}$ is the unit vector in the radial direction. Using thermodynamic arguments Barbero et al showed that f_0 is of the same order of magnitude as the flexoelectric coefficients of a nematic.

The contributions to the total Helmholtz free energy F will be the following. First, the usual elastic free energy density, f_{elas}, of the form

$$f_{elas}=\frac{K}{2}\left[(\nabla\cdot\hat{n})^2+(\nabla\times\hat{n})^2\right], \tag{20}$$

where $K\equiv K_1=K_2=K_3$ is the elastic constant in the equal constants approximation. Then the contribution due to the applied external fields, f_{elec}, is

$$f_{elec}=-\frac{1}{2}[\epsilon_a^{opt}(1+\zeta)E_o^2\sin^2\theta+\epsilon_a^{stat}E_s^2\cos^2\theta], \tag{21}$$

where ϵ_a^{opt} and ϵ_a^{stat} denote, respectively, the dielectric anisotropies for the optical and low frequency fields. They have the form $\epsilon_a\equiv\epsilon_{\|}-\epsilon_{\perp}$ where $\epsilon_{\|}$, $\epsilon_{\perp}$ denote the dielectric constants parallel and perpendicular to the long axis of the molecules. ζ is the amplification factor due to the Janossy effect associated with the dichroic ink and takes into account the additional torque provided by the dye doped liquid crystal. Finally, if we restrict ourselves to contributions quadratic in both fields, the order electric polarization energy density is given by

$$f_{ord}^{ac}=\frac{1}{2}\boldsymbol{P}_{ord}\cdot\boldsymbol{E}_{ac}. \tag{22}$$

From the expression for $\boldsymbol{P}_{ord}$, equation (19), the explicit form of f_{ord}^{ac} is found to be

$$f_{ord}^{ac}=f_0\gamma(r)\frac{dT}{dr}\sin 2\theta \tag{23}$$

and therefore

$$F=\int_V(f_{elas}+f_{elec}+f_{ord}^{ac})d\overrightarrow{r}. \tag{24}$$

Note that f_{ord}^{ac} is proportional to $|E_{opt}^2|^2$through $\partial T/\partial z$, since in the heating equation (10) the source of the temperature profile is the optical field. If an explicit coupling of $\boldsymbol{P}_{ord}$ with the total field $\boldsymbol{E}_{ac}+\boldsymbol{E}_{opt}$ were allowed, it would generate cubic terms in the fields which are higher order terms beyond the quadratic approximation we are considering. The fact that thermal effects are important, as we have taken into account by the order polarization term f_{ord}^{ac}, makes plausible to consider condensation free energy terms arising from a Landau-de Gennes expansion in a power series of the order parameter. However, following Barbero et al., we have restricted our model up to second powers of the order parameter to describe the coupling between order parameter, director and external fields. A Landau-de Gennes type of analysis would allow us to elucidate theoretically whether or not a phase transition exists, but in this work that assumption is taken for granted on the basis of the experimental observations already described.

As is usual in the description of reorientation in thin films, we now assume that the reorientation between the initial and final equilibrium orientational configurations is a relaxation process of the form

$$\frac{\partial\theta(z,r,\phi,t)}{\partial t}=-\frac{1}{\eta}\frac{\delta F}{\delta\theta}, \tag{25}$$

where ϕ is the azimuthal angle, η is the orientational viscosity and $\delta F/\delta\theta$ stands for the variational derivative of F. From the corresponding Euler-Lagrange equation we find that for this model the reorientation equation, which represents the torque balance in the system, turns out to be

$$\frac{\partial\theta}{\partial t}=D\nabla^2\theta+\frac{1}{2}g\,(r)\sin 2\theta+h\,(r)\cos 2\theta, \tag{26}$$

where $D\equiv K/\eta$ is the ratio between the elastic constant K and the orientation viscosity η. The functions and $g\,(r)$ and $h\,(r)$ are given, respectively, by

$$g(r)\equiv\eta^{-1}2\left[\Gamma(r)-E_s^2\epsilon_{as}\right], \tag{27}$$

with

$$\Gamma(r)\equiv E_o^2e^{-\left(\frac{r}{\sigma}\right)^2}, \tag{28}$$

and

$$h\,(r)\equiv\eta^{-1}2\gamma(r)\frac{\partial T}{\partial r}. \tag{29}$$

Note that in this expression both, the function, $\gamma(r)=dS/dT$ and the magnitude of the temperature gradient $\partial T/\partial r$, are unknown functions of r. In the next section we propose an approximate approach to solve equation (26) which allows us to estimate both functions.

4 Approximate separable solutions

In order to determine the r dependence of $h\,(r)$, the unknown function $\gamma(r)$ has to be modeled according to the type of solution of equation (26) that we look for. From here on we shall restrict ourselves to describe only the early stages of the reorientation process where θ remains small ($\theta\approx 0$) and therefore equation (26) reduces to

$$\frac{\partial\theta}{\partial t}=D\,\nabla^2\theta+g\,(r)\;\theta+h\,(r)\,. \tag{30}$$

In principle, the boundary conditions at $z=\pm l/2$ allow for a variety of possible solutions of this equation. However, as a consequence of the asymmetry of the system, the experimental results show that the observed diffraction pattern presents an angular dependence which is nearly independent of the radius. This suggests that the angular

dependence of the solution is independent of the radial part and therefore it is reasonable to propose a separable solution of the form

$$\theta(r,z,\varphi,t) = v(z)\, w(r)\, u(\phi,t). \tag{31}$$

Consequently, equation (30) becomes

$$\frac{\partial u}{\partial t} = \frac{D}{r^2}\frac{\partial^2 u}{\partial \varphi^2} + \frac{Du}{v}\frac{d^2 v}{d\, z^2} + \frac{Du}{w}\frac{d^2 w}{dr^2} + \frac{Du}{rw}\frac{dw}{dr} + g\,(r)\; u + \frac{h\,(r)}{vw}. \tag{32}$$

This equation has no exact solutions for $v(z)$, $w\,(r)$ and $u\,(\varphi,t)$. Nevertheless, approximate meaningful solutions can be obtained if we introduce two assumptions which indirectly take into account the presence of the thermal gradient. The first one is to consider that the value of the parameter $D = K/\eta$ decreases as the temperature rises when $r \to 0$, in such a way that $D = k_0 r^2$, with k_0 a positive constant. This assumption is supported by the fact that for the temperature variations involved in the experiment, the viscosity η remains practically constant, whereas the elastic constant K decreases with temperature. Since Figure 3 shows that approximately $T \sim r^{-2}$ for $r > \sigma/2$, it follows that $D \sim r^2$. The second assumption stems from the observation that $h\,(r)$ is a decreasing function of r, which drops as the thermal gradient vanishes, and $w(r)$ must also drop as $r \to \infty$. Consequently, as a first approximation we rewrite $h\,(r)$ defined by equation (29), in the form $h\,(r) = h_0 k_0 w(r)$, with h_0 a constant. These two assumptions might seem rather stringent and, therefore, they should be validated a posteriori by comparing the predictions of this model with direct experimental observations.

Using the two assumptions mentioned above, equation (32) takes the form:

$$\frac{1}{u}\frac{\partial u}{\partial t} - \frac{k_0}{u}\frac{\partial^2 u}{\partial \varphi^2} - \frac{h_0 k_0}{uv} = \frac{k_0 r^2}{v}\frac{d^2 v}{dz^2} + \frac{k_0 r^2}{w}\frac{d^2 w}{dr^2} + \frac{k_0 r}{w}\frac{dw}{dr} + g\,(r)\,, \tag{33}$$

which implies that $v\,(z)$ is necessarily a constant whose value can be set equal to one. Taking into account that $v = 1$, it can be seen that the l.h.s. of equation (34) depends only on φ and t, whereas the r.h.s. depends only on r, and consequently each member must be equal to a constant. If this constant is written in the form $k_0 m^2$, equation (33) implies that $u(\varphi,t)$ and $w(r)$ are defined, respectively, by the following equations

$$k_0^{-1}\frac{\partial u}{\partial t} = \frac{\partial^2 u}{\partial \varphi^2} + m^2 u + h_0, \tag{34}$$

$$r^2\frac{d^2 w}{dr^2} + r\frac{dw}{dr} - \left[m^2 - k_0^{-1} g\,(r)\right] w = 0. \tag{35}$$

Owing to the Gaussian nature of the laser beam, far from its center $g(r)$ tends to a constant value, which can be written as $k_0 g_0$. Therefore, for $r > \sigma$, the last equation (35) can be approximated as

$$r^2\frac{d^2 w}{dr^2} + r\frac{dw}{dr} - L^2 w = 0, \tag{36}$$

where $L^2 \equiv m^2 - g_0$. As we shall see in the following, from equations (34) and (36) we can infer some of the observed features of the behavior of the diffraction pattern discussed in the previous section.

Let us consider the time-independent solutions first. From equation (34) it follows that in the stationary states $u(\varphi)$ is described by the equation

$$\frac{d^2 u}{d\varphi^2} = -\frac{d}{du}\left(\frac{1}{2}m^2 u^2 + h_0 u\right), \tag{37}$$

which can be visualized as the equation of motion (with φ in the role of time) of a particle of unitary mass moving under the action of a quadratic potential. Since the general solution of this equation is

$$u(\varphi) = \frac{c_1}{m^2}\sin(m\varphi) + \frac{c_1}{m^2}\cos(m\varphi) - \frac{h_0}{m^2} \tag{38}$$

with $c_i \in \mathbb{R}$, the director's orientation will be a periodic function of the azimuthal angle φ and it will present $2m$ extrema within the interval $0 < \varphi < 2\pi$.

Concerning the radial equation (36), it is clear that there are two linearly independent solutions of the form r^L and r^{-L}. The linear combinations of these solutions [i.e., functions of the form $w(r) = a_1 r^L + a_2 r^{-L}$, with $a_i \in \mathbb{R}$] diverge for $r \to 0$ and/or $r \to \infty$, and so they are not physically acceptable since they are not consistent with the initial hypothesis that $\theta = v(z)\, w(r)\, u(\varphi,t)$ remains small. However, if we widen the solution universe of equation (34) and we take into consideration weak solutions with discontinuous derivatives, we can arrive at physically meaningful solutions. To this end we must observe that equation (35) accepts continuous solutions with discontinuous derivatives (peaked solutions) at a point r_0 only if the following jump condition is satisfied

$$[w'] = -\frac{1}{r_0}\,[w']\,, \tag{39}$$

where $[w']$ denotes the change in the value of the derivative $w'(r)$ as we cross the point r_0, i.e., $[w'] \equiv \lim_{\varepsilon\to 0}[w'(r_0+\varepsilon) - w'(r_0-\varepsilon)]$, and $[w'']$ is similarly defined. Peaked solutions of equation (35) which do not diverge at $r = 0$ nor at $r = \infty$, can be constructed in the following way

$$w(r) = a\, H(r_0 - r)\, r^L + b\, H\,(r - r_0)\; r^{-L}, \tag{40}$$

where $a, b, r_0 \in \mathbb{R}$ and $H(r)$ is the Heaviside unit function. This function is continuous at r_0, satisfies the jump condition (39) if $b = a\, r_0^{2L}$ and preserves the ring structure of the pattern if $L \sim 3.5$. It should be recalled that we have assumed that $h\,(r) = h_0 k_0 w(r)$ and that, on the other hand, from equation (29) we know that

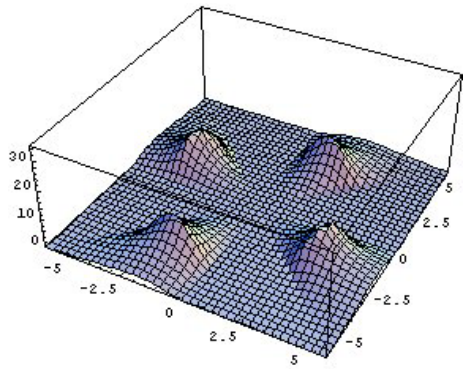

Fig. 4. Shape of the function for $m = 4$, $L = 3.5, ...$

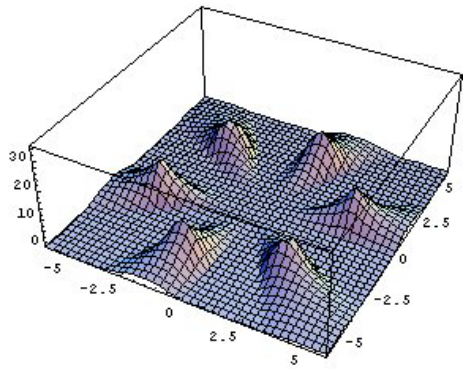

Fig. 5. Same as in Figure 4 for $m = 6, ...$

$h(r) \equiv \eta^{-1} 2\gamma(r) \frac{dT}{dr}$. Then, from equations (29) and (40) we can determine $\gamma(r)$. In the following we shall see that a solution of the form (40) is consistent with the observed diffraction patterns. Note that equations (38) and (40) imply that the equation (33), which describes the behavior of the director´s orientation, has approximate stationary solutions with the following structure

$$\theta(r,\phi) = w(r)\, u(\phi) = \left[\frac{c_0}{m^2}\, \sin\,(m\phi) - \frac{h_0}{m^2}\right] \times \left[a\, H\,(r_0 - r))\; r^L + b\, H\,(r - r_0)\; r^{-L}\right]. \quad (41)$$

The form of this function for $L = 3.5$, $r_0 = 4$, $a = 0.1$, $b = a\, r_0^{2L}$, $c_0 = m^2$, $h_0/c_0 = 1.2$, $m = 4$ and $m = 6$ is shown, respectively, in Figures 4 and 5.

When a laser beam crosses orientational structures like those seen in Figures 4 and 5, Fraunhofer diffraction patterns are produced. These patterns are given by the Fourier transform of the function (41). In particular, the Fourier transform of the function presented in Figure 4 can be seen in Figure 6. This figure exhibits two outstanding features: a set of nearly circular concentric rings, and superimposed to these rings a structure which resembles the vanes of a windmill. As the diffraction patterns observed in the laboratory really presented both of these features, the approximate equation (32) and its proposed separable solution (31) are indeed able to catch some of the essentials of the nematic´s dynamic diffraction pattern behavior.

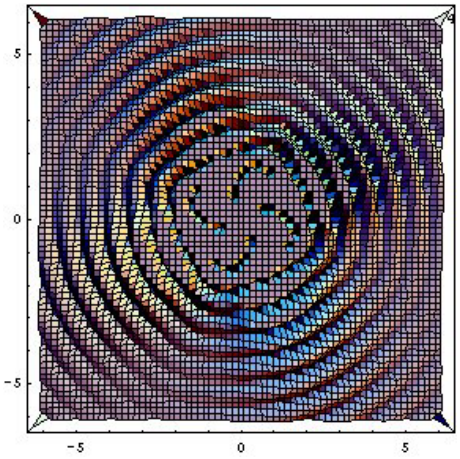

Fig. 6. Fourier transform (i.e., the diffraction pattern) of the function shown in Figure 4.

Now let us consider the time-dependent solutions. Equation (34) has nonstationary solutions of the form:

$$u(\varphi,t) = \frac{c_1}{m^2}\, e^{-pm(\varphi-\omega t)} \sin\left[qm\,(\varphi - \omega t)\right] - \frac{h_0}{m^2}, \quad (42)$$

where $p = \omega/\,(2k_0 m)$, $q = \left(1 - p^2\right)^{1/2}$ and c_1 is a constant which depends on the initial conditions. This function is not periodic in φ, which is physically unacceptable. However, if we restrict the domain of this function to the interval $0 < \varphi < 2\pi$, and we impose the necessary boundary condition $\varphi(0,t) = \varphi(2\pi,t)$, the following condition is obtained:

$$\omega^2 = 4k_0^2\left(m^2 - n^2\right), \quad (43)$$

where $1 \le n \le m$ is an integer. This equation is interesting: it implies that the frequency can be positive or negative, and it has a maximum value $\omega_{max} = 2k_0(m^2-1)^{1/2}$ which depends on the parameter m (the number of vanes in the windmill-structure seen in the diffraction pattern). If $n = m$ the frequency is zero and we recover an stationary solution of the form (38). Since the parameter k_0 was introduced through the approximation $D\,(r) = k_0 r^2$, and for $r > \sigma/2$ we expect $D\,(r)$ to have a value close to K/η, a reasonable upper bound for k_0 is $4K_0/\sigma^2\eta$, thus implying that $\omega_{max} = 8K_0(m^2-1)^{1/2}/\sigma^2\eta$, or equivalently:

$$\nu_{max} \equiv \frac{\omega_{max}}{2\pi} = \frac{4K_0}{\pi\sigma^2\eta}(m^2-1)^{1/2}. \quad (44)$$

If we take, for example, $\sigma = 31\ \mu$m, $\eta = 4\times10^{-7}$ poise and $K = 10^{-11}$ N (which are typical values for the viscosity and the elastic constant of a liquid crystal), equation (44) implies that $\nu_{max} = 3.3\left(m^2-1\right)^{1/2}$ Hz. In particular, if $m = 2$, this maximum frequency turns out to be $\nu_{max} = 5.7$ Hz, which quite is of the same order of magnitude than the value found in the laboratory, $\nu_{\rm exp} = 2.58$ Hz.

5 Discussion

In this work we have proposed a model to analyze some of the effects induced on the diffraction pattern produced

by the simultaneous action of an optical and an AC electric field on a thin, doped nematic film in the SR regime. The basic physical mechanism underlying the model is the heating produced by the laser beam and its interplay with the reorientation process of the director. It should be stressed once again that our model is restricted to considering free energy densities quadratic in the applied fields. Also, since according to the experimental observations an isotropic phase is present for $r \leq \sigma$, the consideration of an expansion of the Landau-de Gennes type is unnecessary.

We proposed a heating model to describe the temperature profile in the stationary state and introduced two assumptions: one concerning the radial dependence of D and the other one specifying the behavior of $h(r)$ which amounted to model $\gamma(r)$. These assumptions allowed us to set up a closed reorientation equation which admits separable solutions. This solution predicts an angular velocity of the pattern that is in quite a good agreement with our measured value of the same quantity. On the one hand, this agreement suggests that the proposed picture of thermally induced tilted nematic domains surrounding the isotropic droplet, is a plausible physical model; on the other hand, it validates the two specific and rather stringent assumptions on the behavior of $h(r)$ made in Section 3. Once $h\,(r) = h_0 k_0 w(r)$ is determined, $\gamma(r)$ can be obtained from equation (29). Since to our knowledge the function $\gamma(r)$ has not been measured, this way of determining it was convenient and consistent.

To our knowledge, the existence of the observed dynamic regimes in the dynamic diffraction pattern described here has not been reported before in the literature. Perhaps the reason is that fields producing comparable torques had not been used so far.

Clearly, it is essential to point out that it is necessary to characterize in a better and more precise way the numerous and complex phenomena involved in the behavior of the pattern, such as the hydrodynamic backflows which are inevitably produced during the reorientation process; or the hysteresis in the response, the linear and non linear dye absorption effects, etc., all of which have been entirely neglected in this preliminary model in spite of their obvious importance. Also, a more detailed study to characterize experimentally the other observed dynamic regimes is needed.

R.F.R. acknowledges partial financial support from grant DGAPA-UNAM IN108006 and from FENOMEC through grant CONACYT 400316-5-G25427E, Mexico.

References

1. B.Ya. Zel'dovich, N.F. Pilipotskii, A.V. Sulchov, N.V. Tabiryan, JETP Lett. **31**, 363 (1980)
2. A.S. Zolotko, V.F. Kitaeva, N. Kroo, N.N. Sobolev, A.P. Sukhorukov, V.A. Troshkin, L. Czillag, Sov. Phys. JETP **60**, 488 (1984)
3. G. Cipparrone, V. Carbone, C. Versace, C. Umeton, R., Bartolino, Phys. Rev. E **49**, 2957 (1994)
4. V. Carbone, G. Cipparrone, C. Versace, C. Umeton, R. Bartolino, Mol. Cryst. Liq. Cryst. A **299**, 91 (1997)
5. E. Santamato, G. Abbate, P. Maddalena, L. Marrucci, D. Paparo, B. Piccirillo, Mol. Cryst. Liq. Cryst. **328**, 479 (1999)
6. E. Santamato, G. Abbate, P. Maddalena, L. Marrucci, Y.R. Shen, Phys. Rev. Lett. **64**, 1377 (1990)
7. M.I. Barnik, et al. Mol. Cryst. Liq. Cryst. **299**, 91 (1997)
8. G. Demeter, L. Kramer, Phys. Rev. Lett. **83**, 4744 (1999)
9. I. Jánossy, Phys. Rev. E, **49**, 2957 (1994)
10. J.A. Olivares, Ph.D. Dissertation, Universidad Nacional Autónoma de México, 2004 (in Spanish)
11. J.A. Olivares, J.A. Reyes, R.F. Rodríguez, F.L.S. Cuppo, J. Phys. IV (Paris) **125**, 479 (2005)
12. L.M. Blinov, V.G. Chigrinov, *Electrooptic Effects in Liquid Crystal Materials* (Springer-Verlag, New York, 1996)
13. I. Jánossy, T. Kósa, Mol. Cryst. Liq. Cryst. **207**, 189 (1991)
14. H.S. Carlslaw, T.C. Jaeger, *Conduction of Heat in Solids* (U. P. Oxford, Oxford, 1959)
15. R.B. Meyer, Phys. Rev. Lett. **22**, 319 (1969)
16. J. Prost, J.P. Marcerou, J. Phys. (Paris) **38**, 315 (1977)
17. G. Barbero, I. Dozov, J.F. Palierne, G. Durand, Phys. Rev. Lett. **56**, 2056 (1986)
18. I.C. Khoo, S.T. Wu, *Optics and Nonlinear Optics of Liquid Crystals* (World Scientific, Singapore, 1993)
19. H. Híjar, R.F. Rodríguez, Phys. Rev. E **69**, 051701 (2004)